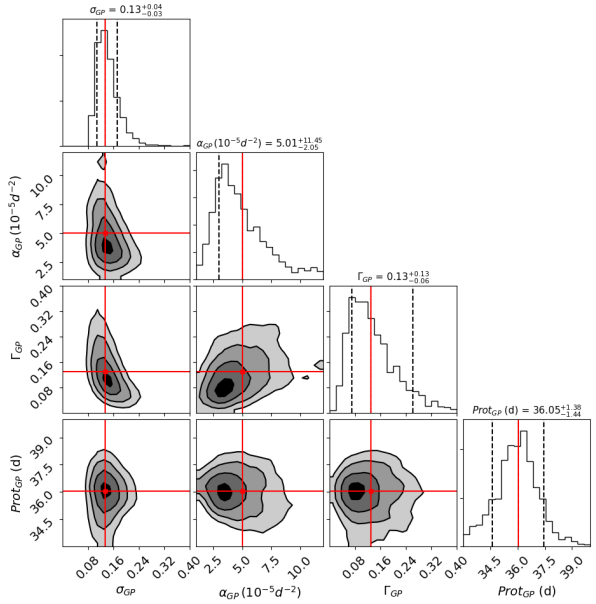

Fig. 8. Posterior distributions for the parameters that model the stellar variability using the S-index activity indicator. The vertical dashed lines indicate the 16, 50, and 84% quantiles of the fitted parameters; this corresponds to 1σ uncertainty. The red line shows the median value of each fitted parameter.

range 35–45 d (purple colored area). In particular the S-index GP regression analysis established the stellar rotation period at $P_{\rm rot} = 36.05^{+1.39}_{-1.44}$ d. We conclude that all the possible signals identified in the RV GLS periodogram around this value could be related to stellar activity effects or to the stellar rotation period and therefore their Keplerian nature can be ruled out. The different activity indicators used here track different features in the stellar atmosphere and considering the differential rotation of the star it is plausible that they do not yield exactly the same periods found in RV data. In fact the closest period that we could identify in the RV GLS periodogram is 42.1 d.

4.3. Photometric stellar activity

The M dwarfs have inhomogeneities on their surface that rotate with the star. These inhomogeneities cause RV variations due to the distortion of the spectral line profile and can be misinterpreted as signals of Keplerian nature. Those inhomogeneities affect also the photometric measurements that is why a photospheric analysis is crucial in order to avoid unwanted signals as planetary candidates.

Super-WASP and MEarth. We analyzed the GLS periodograms of Super-WASP light curve and MEarth differential light curves (*c* and *d* panels of Fig. 4). There are several observing seasons for GJ 720 A within the MEarth survey, thus we studied the differential light curves separately per observing campaign and all the seasons together. Due to the huge number of data points obtained with MEarth we also analyzed the binned differential light curve data. The different analysis for the MEarth available seasons yielded that the variability of the star is better seen in the binned 2008–2010 season, the rest of them are not shown here for clarity. No obvious, significant peak can be extracted from the GLS periodograms of the Super-WASP and MEarth light curves. In both cases, there is no clear and narrow peak which can be attributed to the stellar rotation period. The Super-WASP GLS periodogram of the binned data shows the two highest peaks around 40 and 100 d (panel *c* of Fig. 4). The MEarth GLS periodogram (using the binned data of the season 2008-2010) shows the highest peak around 90 d (*d* panel of Fig. 4) and, after subtracting its contribution (black vertical line of *e* panel of Fig. 4), the highest period moves towards ∼40 d. The periodicities showed in the GLS light curves periodograms agree with those found in the GLS analysis of both RV and spectroscopic activity indicators (light blue and purple colored areas in Fig. 4). No photospheric or spectroscopic activity signal is detected in the region of interest around 19 d.

EXORAP. We first analyze the four differential light curves (one for each band) using the GLS periodogram. As the observed photometry shows long term trends, we pre-whiten the light curves by subtracting from each data series the corresponding third-order polynomial best-fit. The periodogram of the pre-whitened *B* light curve (see panel *f* of Fig. 4) shows two peaks with FAP<1% at ∼34 and ∼140 days. In the *V*, *R* and *I* bands we do not detect any signal more significant than 5% and therefore we do not show them here for clarity. These results suggest a scenario where the photometric variability is due to the effects of an irregularly spotted stellar surface coupled with stellar rotation. This is consistent with the fact that the activity signal is stronger at bluer wavelengths, where the contrast between photosphere and cool spots is larger.

APACHE. Giacobbe et al. (2020) has recently published the GJ 720 A rotation period at 33.6 days using the APACHE differential photometric observations. Using the same APACHE binned photometric data we computed the GLS periodogram here (panel *g* of Fig. 4) corroborating that the highest peak value corresponds to that published. But we consider that such value can be regarded as an approximate rotation period of the star because of the presence of other nearby peaks (e.g., ∼37 days) with a comparable significance. Folding in phase the APACHE light curve at 33.6 d, the amplitude is relatively small (2.5±0.2 mmag) compared with the *rms* of the data (5.5 mmag) and the mean weighted internal errors (3.9 mmag), which explains why this signal can not be clearly identified in the GLS periodogram. Analyzing the different photometric epochs separately we also found the ∼33 and ∼37-d signals as the highest ones in the GLS periodogram of the first and fourth APACHE epochs.

TESS. We looked at the *TESS* light curve using the SAP fluxes to model the stellar activity signatures in order to find a possible stellar rotational period and we used the PDC fluxes for transit searches. The two sectors *TESS* light curves were analyzed at the same time using a quasi-periodic kernel (QPK) introduced by Foreman-Mackey et al. (2017) of the form

$$k_{i,j}(\tau) = \frac{B}{2+C} e^{-\tau/L} \left[\cos\left(\frac{2\pi\tau}{P_{rot}}\right) + (1+C) \right], \quad (2)$$

where $\tau = |t_i - t_j|$ is the time-lag, B and C define the amplitude of the GP, L is a timescale for the amplitude-modulation of the GP, and $P_{\rm rot}$ is the period of the quasi-periodic modulations. The `juliet` lightcurve models include a dilution factor (D_i) which allows to account for possible contaminating sources

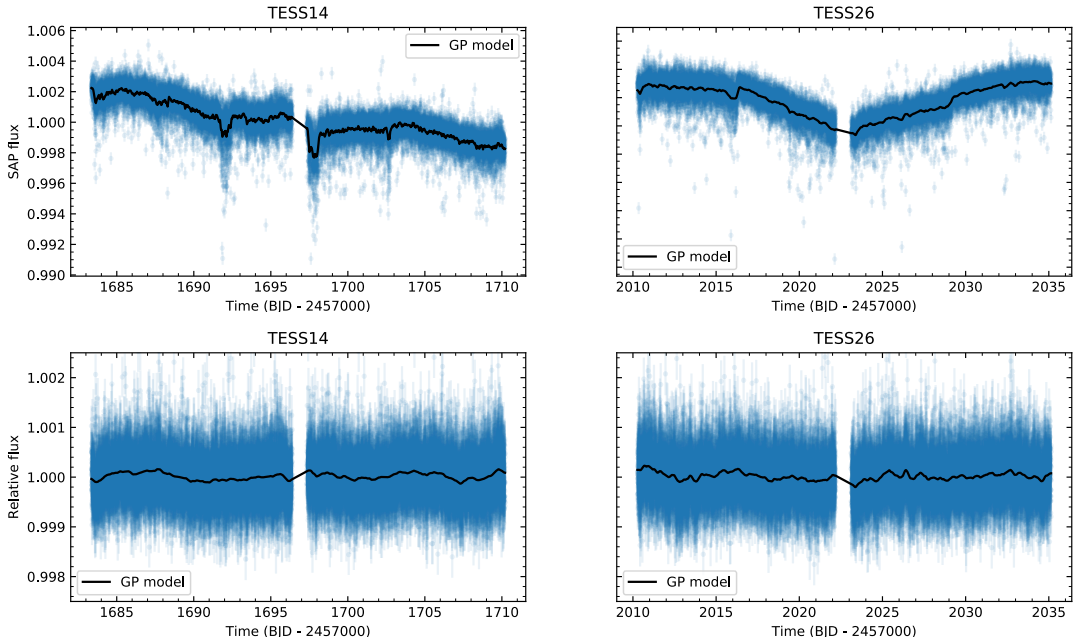

Fig. 9. *Top panel:* GJ 720 A *TESS* SAP fluxes (blue points) for the two sectors with the best stellar activity model (black line). *Bottom panel: TESS* PDC fluxes (blue points) with the best GP model fitted (black line).

in the aperture that might produce a smaller transit depth than the real one. Also the model takes into account the relative out-of-transit target flux (M_i) which is a multiplicative term and not an additive offset. For the transit modeling, `juliet` uses the `batman` package (Kreidberg 2015). The limb-darkening effect was taken into account with q_1 and q_2 coefficients, as defined by Kipping (2013), and a quadratic law. Figure 9 shows the SAP (top panels) and PDC data (bottom panels) for the two *TESS* sectors with the best GP model found. In our case the median value of the posterior distribution for the rotational period for the two *TESS* different sectors using the SAP fluxes is $49.8^{+7.3}_{-11.5}$ and $28.9^{+16.0}_{-7.1}$ d, respectively. While using the PDC fluxes the median values of the rotational period for the different sectors is $33.7^{+11.0}_{-15.9}$ and $34.8^{+10.1}_{-13.8}$ d, respectively. The corresponding error bars in both cases (SAP and PDC fluxes) are slightly high which suggests that there is not a precise determination of the rotation period for GJ 720 A star when using the *TESS* photometric data. *TESS* time series are shorter than the period we are looking for. Therefore, searching for the rotation period with *TESS* data is not providing precise results. But the obtained values agree with those obtained before when analyzing the rest of spectroscopic and photometric activity indicators.

A GP model can be also used in order to detrend the *TESS* light curves before the search of possible transit features. Therefore using the optimized PDC fluxes and the corresponding previous GP model fit to detrend the light curve, we proceed to search transits. In a first approach searching possible transits we set a wide uniform prior, 1–25 d, for the planetary signal. In a second approach we took advantage from the times of the inferior conjuctions as derived from the RV curve, in order to estimate the expected times of the transits and to look specifically at those times in the *TESS* light curves. In both approaches no transiting planets for GJ 720 A were found.

We can conclude after the chromospheric and photospheric analysis that all activity indicators show a significant but broad peak, always in the range of 35–45 d. Therefore, this range can be associated with stellar active regions probably at different latitudes on a differentially rotating star. In fact the GP analysis with the S-index revealed the stellar rotation period to be $P_{\rm rot} = 36.05^{+1.39}_{-1.44}$ d. While the other identified signal by the activity indicators (also seen in RV data) at around 100 d is more likely related to the life cycle of the active regions, as explained by Scandariato et al. (2017) where was established that the active regions could persist some stellar rotations. Due to the complex mechanism that the differential rotation can exhibit on M dwarf stars due to their convective layers, we could not find a narrow signal that determines a precise value for the rotation period in each one of the analyzed activity indicators.

5. Gaussian process regression

The impact that the stellar activity effects can induce in the RVs could be different as a function of the stellar magnetic phenomena (e.g., evolving spot configurations among others). Each target star can have a specfic behaviour for accounting the effects of its stellar variability (e.g., rotating spots, faculae) and the flexibility of the GP algorithms makes their use essential in order to reproduce the stellar phenomena (Perger et al. 2020). However the diversity of the mathematical GP kernels associated with true physical phenomena has not been well evaluated to date. Therefore it could be possible that the stellar activity of a specific target could be explicitly better reproduced by one kernel than by another. We decide in this section to test two of the commonly used kernels (exp-sin-squared and QP) to reproduce the stellar variability in order to obtain a robust result of the planet parameters and to know the goodness of the kernels for this specific target.

Table 3. Comparison of different solutions for GJ 720 A using `juliet`.

Model[(1)]	Params.	Description	ln $\mathcal{L}$	BIC[(2)]
BM	γ_0	RV offset	-394	798
	σ	RV jitter		
BM+GP	$\sigma_{\rm GP}$	Amplitude of GP	-315	660
	$\alpha_{\rm GP}$	Inverse (squared) length-scale		
	$\Gamma_{\rm GP}$	Amplitude of the sine-part		
	$P_{\rm rot,GP}$	Period of GP		
BM+GP+LT	slope	Slope RV data	-312	665
	inter.	Intercept coeff.		
BM+1pl	P, T_0, e, ω, K	Planet params	-346	718
BM+GP+1pl	...	...	-298	650
BM+GP+1pl+LT	...	...	-295	655
BM+2pl	...	...	-319	698
BM+GP+2pl	...	...	-299	667

Notes. [(1)] BM stands for the base model containing RV offsets and jitter. GP corresponds to a quasi-periodic GP kernel and 1pl means one planet model.[(2)] BIC corresponds to the Bayesian Information Criterion.

5.1. Exp-sin-squared kernel, `juliet`

We used a different approach to analyze the HARPS-N RV data in search for planet candidates using `juliet`. This technique foresees a simultaneous fit of the stellar activity and the planetary signals. The stellar activity contamination has a significant effect on the derived planetary parameters and to model both signals (stellar and Keplerian) at the same time through the GP regression is essential. The GP kernel implemented here was the exp-sin-squared kernel, previously used and described by the equation 1. The different implemented models will be judged on the basis of the Bayesian Information Criterion (BIC, Liddle 2007). It is based on the log-evidences (ln $\mathcal{L}$) introducing a penalty term for the parameters used in the model avoiding an overfitting of the data. The BIC value can be described by the equation:

$$\mathrm{BIC} = k\ \ln(n) - 2\ \ln(\mathcal{L}), \tag{3}$$

where n is the number of data points, k the number of free parameters to be estimated, and $\mathcal{L}$ the maximized value of the likelihood function of the model (see Espinoza et al. 2019, for details). The models are better when the BIC value is lower. The ΔBIC threshold for considering one model more probable than another with the BIC criterion correspond to: *i)* ΔBIC = 0–2 not worth more than a bare mention, *ii)* ΔBIC = 2–6 is positive, *iii)* ΔBIC = 6–10 is a strong evidence of preferred, and *vi)* ΔBIC > 10 the model is very strongly preferred.

In a first approach we used a base model (BM, only includes individual offset and RV jitter), plus a GP kernel that we used to model the stellar variations observed in the RV data and when analyzing the stellar activity indicators, already discussed in previous sections. We consider uniform distributions for the σ_{GP} and $P_{\rm rot}$ parameters of the exp-sin-squared GP kernel with the priors set to $\mathcal{U}(0,\ 15)$ m/s and $\mathcal{U}(1,\ 1000)$ d, respectively. For α_{GP} and Γ_{GP} GP parameters we followed a Jeffrey's distributions (Jeffreys 1946) setting the prior values as $\mathcal{J}(10^{-20}, 10^{4})$ d^{-2} and $\mathcal{J}(0.01, 100)$, respectively. We set wide prior values for all these four GP parameters in order to test the stellar variability present in the RV data. The expected result with these wide priors, especially with the $P_{\rm rot}$ prior that includes both highest signals (19.5 and ~40 d) of the RV data, was that the BM+GP model would identify some of them as the $P_{\rm rot}$ value. Surprisingly, the value found for the GP $P_{\rm rot}$ parameter using the HARPS-N RV data corresponds to 38.9±0.05 d which is close to the $P_{\rm rot}$ value found from the S-index ($36.05^{+1.38}_{-1.44}$ d), and it is placed in the same activity region (30–50 d) determined from the other activity indicators. The final posterior distributions obtained with a base model plus a GP kernel are shown in Fig. 10. The length-scale of the GP signal corresponds to a value of ~1000 d (α_{GP}=0.74×10^{-6} d^{-2}) while the obtained amplitude of the GP model is close to the *rms* of the RV data. In order to test if including a linear trend (LT) helps the improvement of the final model we also fitted the RV data considering the BM plus a GP kernel plus a LT.

In the second approach we modeled the BM plus one planet. In order to explore a blind search of the planet period, without taking into account the recovered information from the GLS periodogram of the RV data, we set a wide uniform prior value for the period of the planet, $\mathcal{U}_{P1}(1,\ 50)$ d. This prior includes the highest signals of the RV GLS periodogram (19.5 and ~40 d). The rest of the priors were set as follows: uniform distributions for the eccentricity $\mathcal{U}_{ecc}(0,\ 0.8)$, the argument of periastron $\mathcal{U}_{\omega}(0,\ 360)$ deg, the semi-amplitude $\mathcal{U}_{K}(0,\ 10)$ m/s, and the time of periastron passage $\mathcal{U}_{t_0}(0,\ 50)$ d with respect to the time reference 2,456,000. The period found for the planet candidate was P1 = $19.484^{+0.007}_{-0.006}$ d with a time of periastron passage at $t_0 = 6.05^{+0.53}_{-0.43}$ (BJD - 2,456,400).

In a third approach, our model was composed of the BM, the GP kernel modeling the activity with a uniform distribution of $\mathcal{U}(30,\ 50)$ d for the $P_{\rm rot}$ GP parameter plus one planet with a normal distribution for the planet orbital period of $\mathcal{N}(19.5,\ 0.5)$ d. The same model as the previous one but considering the $P_{\rm rot}$ GP parameter as an open uniform distribution, $\mathcal{U}(1,\ 1000)$ d, was also considered. The planet and GP parameters obtained for these two models were compatible within 1σ error bars. Another test was also considered including a linear trend in the model. We note that the narrow prior adopted here for the planet, $\mathcal{N}_{P1}(19.5,\ 0.5)$ d, is larger than its final posterior distribution and it is also larger than the final posterior distribution obtained following the second approach where we set a wide uniform prior for the planet ($\mathcal{U}_{P1}(1,\ 50)$ d). Therefore the 19.5 d signal is well

characterized and in what follows the assumption of this narrow prior ($\mathcal{N}_{P1}(19.5, 0.5)$ d) is justified.

In the fourth and last approach we considered the two highest RV signals (19.5 and ~40 d) of Keplerian origin. The first model took into account the BM plus two planets. The orbital planetary periods were considered with normal distributions $\mathcal{N}_{P1}(19.5, 0.5)$ d and $\mathcal{N}_{P2}(42.1, 0.5)$ d. The second model took into account the BM plus the same two Keplerian signals (19.5 and ~40 d) plus a GP kernel with a wide uniform prior for the $P_{\rm rot}$ in the range 1–1000 d.

The comparison between the different models together with their log-likelihood and BIC values are summarized in Table 3. After that and following the BIC criterion, the "best" model corresponds to the third approach where together with the base model, an exp-sin-squared GP kernel simulating the stellar contribution and a Keplerian orbit for the planet candidate at 19.5 d were employed. The ΔBIC between the model BM+GP and the model BM+GP+1 planet has a value of 10 for the latter to be strongly preferred. The BIC criterion retains more likely the BM+GP+1 planet model than the star-only model and therefore supports the planetary hypothesis at 19.5 d. The distributions and the corresponding priors used to fit the "best" model are listed in detail in Table A.3. The $P_{\rm rot}$ value derived from the "best" RV+GP model (35.23±0.11 d) is compatible, within 1 σ, with the $P_{\rm rot}$ obtained from the S-index GP analysis ($36.05^{+1.38}_{-1.44}$ d). The amplitude and the length-scale of the GP are $4.44^{+2.32}_{-1.36}$ m/s and 842 d (α_{GP}=1.41×10^{-6} d^{-2}), respectively.

Figure 11 shows the simultaneous fit RV+GP with the "best" model as a function of the time and the planetary signal of GJ 720 A folded in phase with the orbital period. The final orbital parameters of the planet are listed in Table 4. Figure 12 shows the GLS periodogram of the original RVs (green line) and the corresponding RV GLS periodogram of the residuals after substracting the "best" model (blue line). This figure shows how the final model produced an optimal removal of all the signals present in the RV data. The *rms* of the residuals is 1.59 ms^{-1}, around three times smaller than the *rms* (4.19 ms^{-1}) of the original RV data.

In Figure 13 we show the posterior distributions of the fitted parameters, this is one planet plus the stellar activity. The planet, GJ 720 Ab, has a minimum mass of 13.64 ± 0.79 $M_\oplus$ located at a distance of 0.119 ± 0.002 AU from the host star with an orbital period of 19.466 ± 0.005 d. Due to the low eccentricity value obtained and its error bars we can conclude that the eccentricity is compatible with zero and therefore our planetary orbit is circular.

A detailed summary of the hyperparameters and priors values used for all the different models followed with `juliet` are listed in Table A.4. While the final parameter values obtained for each model are summarized in Table A.5.

5.2. Quasi-periodic kernel, `emcee`

For completeness, we also have performed another GP analysis on the BM+GP and BM+GP+1pl models that differ in the adopted covariance function, the chain sampler and in priors definition, which are uninformative (see Tab. A.6). This analysis employs the celerite quasi-periodic kernel, described in equation 2, and the `emcee` (Foreman-Mackey et al. 2013) package based on the affine-invariant ensemble sampler for Markov chain Monte Carlo (MCMC) (Goodman & Weare 2010).

The parameter space is covered by 32 walkers, whose initial positions are randomly selected within the priors boundaries. This choice on the initial position of the walkers requires a burn-in phase to free the chain from very low probability values. Therefore, we have set a chain of 50K steps as burn-in, at the end of which a blob, centered at the maximum probability position, is initialized to feed a second chain. We run the second chain until convergence occurs, i.e. the autocorrelation time of each parameter (see Sokal 1996), evaluated every 10K steps, varies less than 1% and the chain is 100 times longer than the estimated autocorrelation time. Based on this criterion, the chains converged

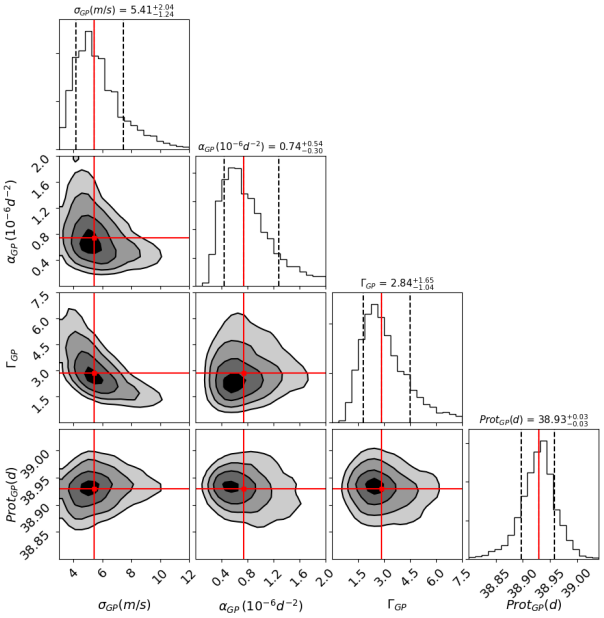

Fig. 10. Posterior distributions for the parameters of the GJ 720 A HARPS-N RV data fitting a base model plus an exp-sin-squared GP kernel setting wide prior values for the GP parameters (e.g., $P_{\rm rot} = \mathcal{U}(1, 1000)$ d).

Table 4. Keplerian orbital parameters of GJ 720 Ab from Gaussian process regression method for the two different approaches that we followed. The first one with `juliet` where the explored parameters were e and ω and the second one using `emcee` where the parameters e and ω are derived from the explored parameters $\sqrt{e}sin(\omega)$ and $\sqrt{e}cos(\omega)$.

Parameter	GJ 720 A b `juliet`	GJ 720 A b `emcee`
P (d)	$19.466^{+0.005}_{-0.005}$	$19.47^{+0.01}_{-0.01}$
T_0 (BJD-2,456,400)[1]	$6.81^{+0.43}_{-0.42}$	$7.02^{+1.63}_{-1.82}$
e	$0.12^{+0.05}_{-0.06}$	$0.10^{+0.06}_{-0.06}$
ω (deg)	$110.22^{+23.97}_{-24.28}$	$102.16^{+29.77}_{-31.48}$
K (m/s)	$4.72^{+0.27}_{-0.27}$	$4.60^{+0.28}_{-0.29}$
γ_0 (m/s)[2]	$-0.53^{+2.29}_{-2.54}$	$0.04^{+0.97}_{-1.04}$
Derived physical parameters		
$m_{\rm p} \sin i$ ($M_\oplus$)	$13.64^{+0.78}_{-0.79}$	
a (au)	$0.119^{+0.002}_{-0.001}$	
$T_{\rm eq}$ (K)[3]	309±24 – 401±32	

Notes. [1] T_0 corresponds to the periastron passage. [2] Arbitrary zero point applied to HARPS-N RVs. [3] For Bond albedo in the interval 0.65–0.0.

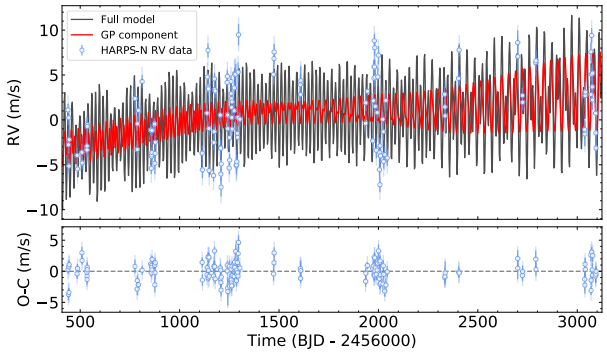

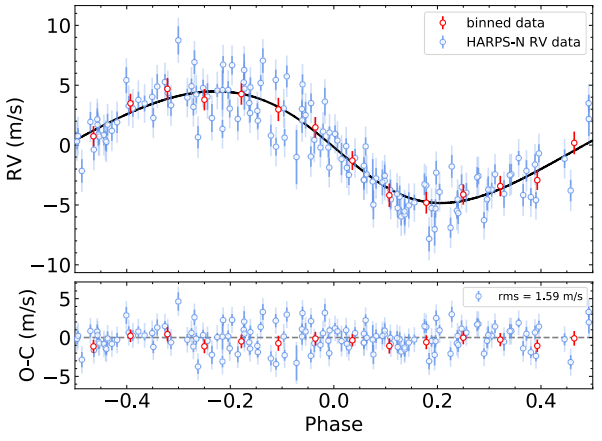

Fig. 11. *Top panel:* RV time series (blue dots) together with the "best" model and the residuals. The fitted model (black line) corresponds to the base model plus an exp-sin-squared GP kernel that models the stellar activity at P_{rot} = 35.23 ± 0.11 d, and the planetary signal at 19.466 ± 0.005 d. The GP contribution is shown with red colored line. The error bars (color blue) include the RV jitter (light blue color) taken into account. *Bottom panel:* RVs (blue dots) folded in phase (the base model and the stellar activity were removed) with the orbital period of the planet and its residuals. The best Keplerian solution (black line) has an RV amplitude of 4.72 ± 0.27 ms^{-1}. The red dots correspond to the binned data. The *rms* of the residuals is 1.59 ms^{-1}.

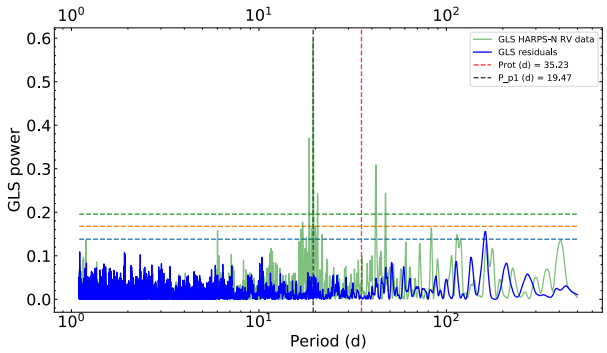

Fig. 12. GLS periodograms of the RV data (green line) and the GLS of the residuals (blue line) after substracting the "best" model that models the RV stellar activity (P_{rot} = 35.23 ± 0.11 d) and the Keplerian signal (19.466±0.005 d) at the same time. The horizontal dashed lines indicate FAP levels of 10% (blue), 1% (orange), and 0.1% (green). The black and red vertical dashed lines indicate the orbital rotational period of the planet and the rotation period of the star, respectively.

Table 5. Comparison of the planetary parameters for the two different observed seasons analyzed and the full dataset using `emcee`. SIII corresponds to the RV data in the range ~[588, 888] days (BJD-2,456,000) and SIV stands for RV data ~[1238, 1638] days (BJD-2,456,000).

Parameter	SIII	SIV	Full Dataset
P (d)	$19.52^{+0.07}_{-0.07}$	$19.35^{+0.16}_{-0.17}$	$19.47^{+0.01}_{-0.01}$
K (m/s)	$5.26^{+0.40}_{-0.41}$	$5.65^{+0.52}_{-0.54}$	$4.60^{+0.28}_{-0.29}$
e	$0.11^{+0.08}_{-0.07}$	$0.13^{+0.10}_{-0.09}$	$0.10^{+0.06}_{-0.06}$
ω (deg)	$165.01^{+43.11}_{-36.97}$	$77.34^{+64.58}_{-34.58}$	$102.16^{+29.77}_{-31.48}$

after 160K and 440K steps, respectively, for the BM+GP and BM+GP+1pl models.

Posterion distributions of the latter model is presented in Fig. 14. BIC parameters for the two models are 766.3 and 649.5, with the lowest being that of the BM+GP+1pl model. As in the previous analysis, the BIC comparison supports the model in which RV data are described with a Keplerian signal whose planetary parameters are in agreement with the ones obtained in the previous analysis and reported in Tab. 4.

5.3. Observing seasons analysis

Looking at the time cadence of the observations we can identify five different observing seasons for our HARPS-N RV data. Only the third and fourth seasons (SIII ~[588, 888] and SIV ~[1238, 1638] days (BJD-2,456,400)) have a significant number of observations in order to investigate the stability of the planetary signal by applying a GP analysis. Priors of BM+GP+1pl model using the `emcee` analysis have been adopted, except for the parameter T_0 whose prior is (BJD-2456400) [0,30]. The estimated planetary parameters for the two subsets are presented in Tab. 5. Obtained values are generally in agreement with respect to the estimates from the former analysis within 1σ confidence. This does not apply to the semi-amplitude (K_1) of the planetary signal which is systematically larger than the one obtained previously and, in the case of SIV, it is compatible with the previously estimated value within 1.3σ. This effect is related to the inability of the quasi-periodic kernel to model the stellar activity in these two seasons, therefore, being the kernel parameters not well constrained, a fraction of the stellar signal is absorbed by the semi-amplitude producing larger values of this parameter.

Looking at the two different posterior distributions obtained with each kernel (exp-sin-squared kernel in Fig. 13 and QP kenel in Fig. 14), we conclude that the exp-sin-squared kernel is the optimal kernel for our target in order to model the stellar variability. The exp-sin-squared kernel is able to identify the same stellar rotational period in the RV data as that obtained from the activity indicators even setting a wide range prior for the GP P_{rot} parameter.

6. Summary and conclusions

The monitoring of GJ 720 A M dwarf with the HARPS-N spectrograph during our observing campaign within the HADES program resulted in a sub-Neptune mass detection of a minimum mass of $13.64^{+0.78}_{-0.79}$ $M_\oplus$ with a semi-major axis of $0.119^{+0.002}_{-0.001}$ AU in a circular orbit ($e = 0.12^{+0.05}_{-0.06}$) that revolves with a period of

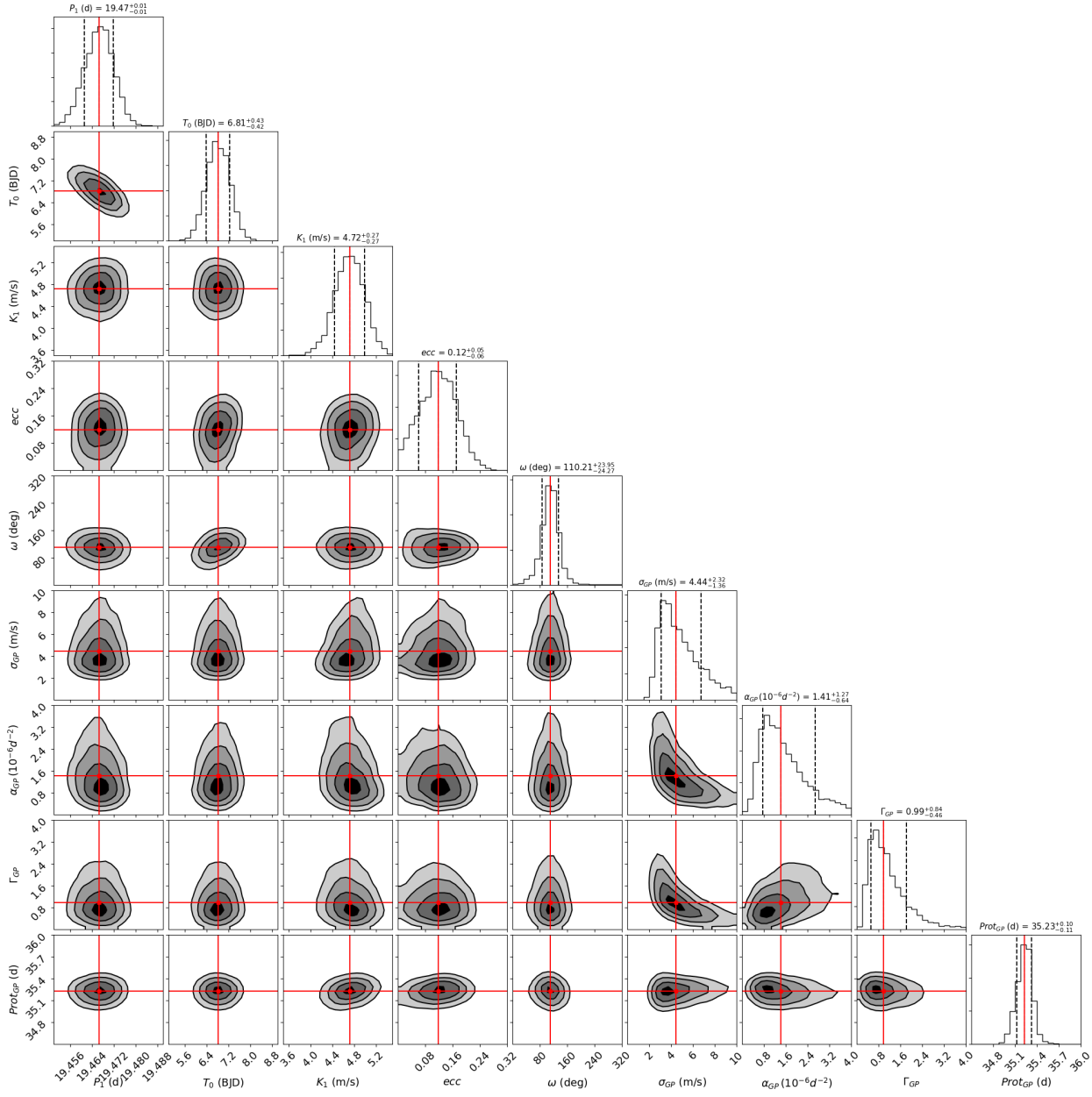

Fig. 13. Posterior distributions for the parameters of the "best" fitted model (BM+GP+1pl) that describes the planet orbiting GJ 720 A and the stellar variability using `juliet`. The vertical dashed lines indicate the 16, 50, and 84% quantiles of the fitted parameters; this corresponds to 1σ uncertainty. The red line shows the median value of each parameter.

$19.466^{+0.005}_{-0.005}$ d. All spectroscopic activity indicators (Hα, Ca II H & K, NaD lines) together with the available photometry from the MEarth, SuperWASP, EXORAP, APACHE, and *TESS* surveys indicate that the other two detected periodicities (∼40 and ∼100 d) in the HARPS-N RV data are related to stellar activity phenomena. In fact the stellar rotation period derived here from the S-index activity indicator using a GP regression determined its value at $P_{\rm rot} = 36.05^{+1.38}_{-1.44}$ d (compatible, within the error bars, with the $P_{\rm rot}$ value (35.23 ± 0.11 d) obatined from the best fit RV data analysis). The RV signal around 100 d is more likely related to a life cycle of the active regions that persists for some stellar rotations. The different approaches we followed here provided strong arguments in favor of the GJ 720 Ab planet detection. No counterparts in any stellar activity indices were found at the planet orbital period, the stability and the coherence of the planetary signal indicates a long-lived behaviour, and the activity and planetary signals are not related with each other by a possible alias phenomena. Also we modeled the stellar variability and the possible Keplearian signals in a simultaneous way using a GP regression and employing two independent analyses (`juliet` and `emcee`) for completeness. We analyzed different possible models (e.g., only GP, GP+1pl, GP+2pl, only Keplerian signals) that

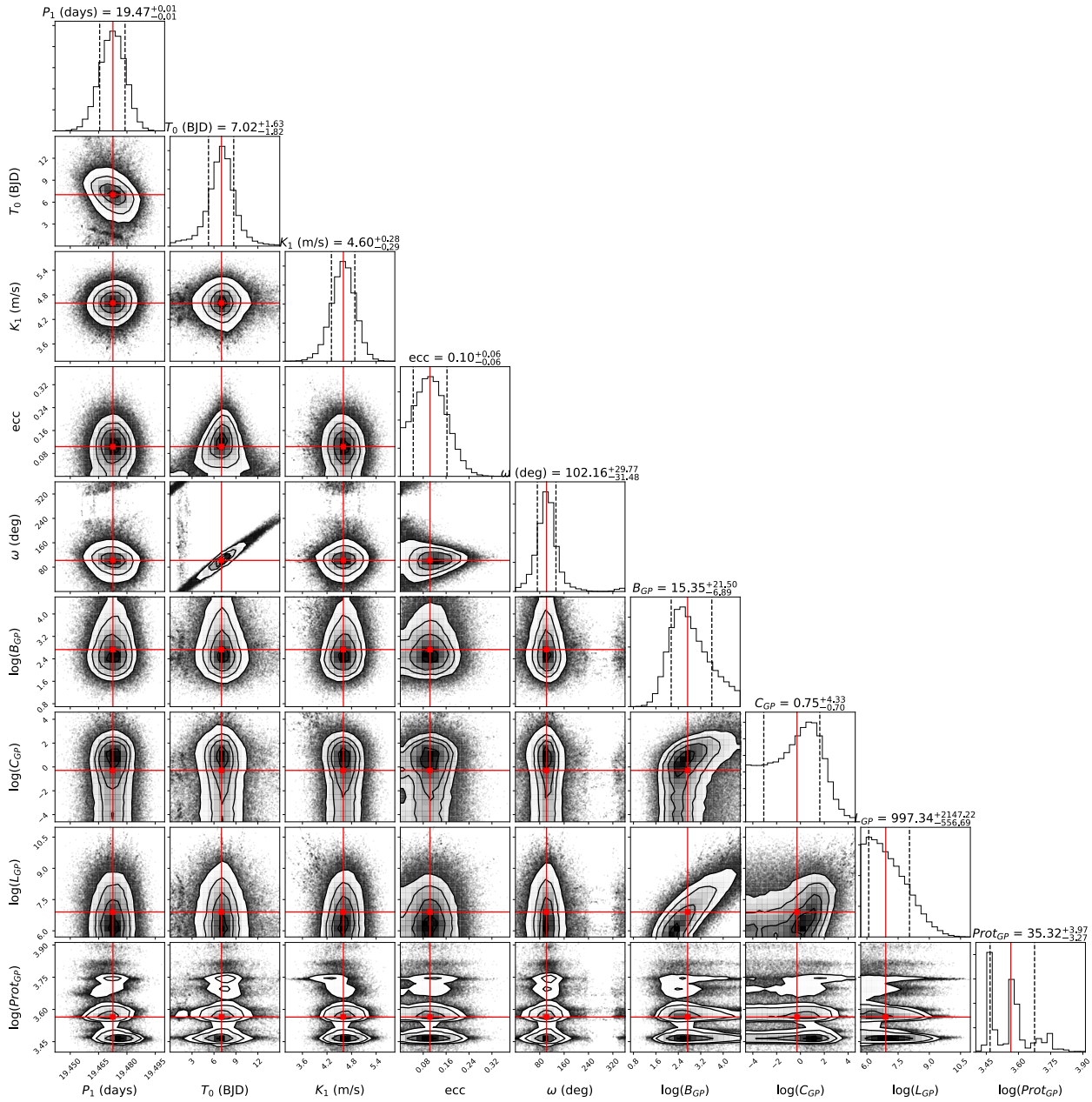

Fig. 14. Posterior distribution of the BM+GP+1pl model in which one sample from the chain over 100 have been displayed. To lighten the visualization, the offset and jitter parameters have not been displayed. The median value of each parameter is plotted with the red line. The results were obtained using `emcee` code. The log describing the GP parameters stands for neperian logarithm

.

could reproduced the RV signals. The one planet model at 19.5 d plus a GP kernel modeling the stellar activity was the fit statistically preferred among the different implemented models and was the fit that determined the final planetary orbital parameters.

We looked at the Kervella et al. (2019) catalog of proper motion anomalies in order to find possible evidence of outer, massive companions in the Hipparcos-Gaia absolute astrometry. There is no statistically significant proper motion variation reported for GJ 720 A. Based on the analytical formulation of Kervella et al. (2019), the sensitivity curve for the star implies that companions with masses of 0.27 M_J at 1 AU are ruled out, and massive planets with a few Jupiter masses, or larger, would produce detectable effects out to a few tens AU. At the exact separation of GJ 720 Ab the detectable mass from proper motion anomaly is found to be around 15 M_J.

In Figure 15 we represent the position occupied by GJ 720 Ab in the diagram of known Neptune-type and super-Earth planets discovered only with the RV method around M dwarfs. From this diagram we can observe that more massive planets are located around early-M dwarfs (blue dots) while the

Earth-like planets are found around mid/late-M spectral type (red/orange dots). We note that could be a selection effect because smaller planets can be detected more easily around smaller stars. Our target populates the more massive sub-Neptune part of the diagram at intermediate orbital periods. Thanks to unbiased fore-casting model presented by Chen & Kipping (2017), we predicted the planetary radius as $3.84^{+1.53}_{-1.44}$ $R_\oplus$. Once obtained an estimation of the planet radius we can derive the probability that GJ 720 Ab transits in front of the disk of its host star and the depth that the planet would infer. The corresponding values correspond to $2.2^{+2.5}_{-1.9}$% of transit probability and 4575^{+7105}_{-3016} (ppm) for the transit depth.

Following the models by Kopparapu et al. (2013, 2014) we estimated the conservative habitable zone limits following the Runaway Greenhouse for 5 $M_\oplus$ coefficients. The received effective stellar flux compared to the Sun corresponds with $S_{\rm eff}$ = 1.01 $S_\odot$ and the inner edge of the GJ 720 A habitable zone is placed at 0.24 AU. The habitable zone determination, following Kopparapu et al. (2014), implies that GJ 720 Ab lies inside the inner boundary of the habitable zone where the insolation flux has a value of $4.28^{+1.25}_{-0.97}$ $S_\oplus$. The theoretical equilibrium temperature ($T_{\rm eq}$) of GJ 720 Ab was derived by using the Stefan–Boltzmann equation, the stellar parameters of Table 1, and two extreme values of the albedo. In the two extreme cases, A = 0.0 and A = 0.65, the $T_{\rm eq}$ for GJ 720 Ab is 401±32 K for a non-reflecting planet and 309±24 K for the high-reflectance planet.

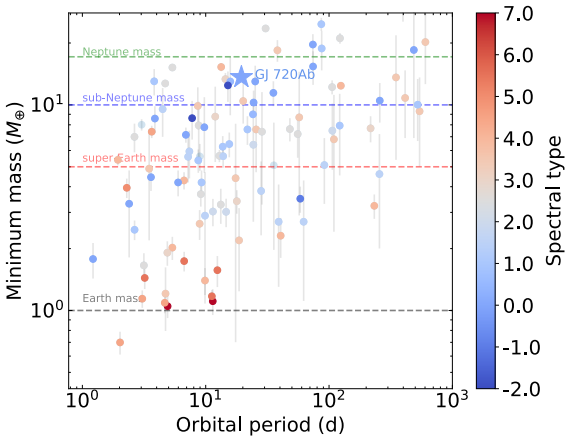

Fig. 15. Minimum mass vs. orbital period diagram for known Neptune-type and super-Earth planets (colored dots) around M dwarfs only detected with RV method (available data at http://www.exoplanet.eu). The star symbol indicates the location of the planet GJ 720 Ab. The colorcode divides the sample by the spectral type of the host star with -2.0, 0.0 and 7.0 corresponding to K5.0V, M0.0V, and M7.0V, respectively.

Acknowledgements. This research was supported by the Italian Ministry of Education, University, and Research through the PREMIALE WOW 2013 research project under grant *Ricerca di pianeti intorno a stelle di piccola massa*. This paper makes use of data from the MEarth Project, which is a collaboration between Harvard University and the Smithsonian Astrophysical Observatory. The MEarth Project acknowledges funding from the David and Lucile Packard Fellowship for Science and Engineering and the National Science Foundation under grants AST-0807690, AST-1109468, AST-1616624 and AST-1004488 (Alan T. Waterman Award), and a grant from the John Templeton Foundation. This work has made use of data from the European Space Agency (ESA) mission *Gaia* (https://www.cosmos.esa.int/gaia), processed by the *Gaia* Data Processing and Analysis Consortium (DPAC, https://www.cosmos.esa.int/web/gaia/dpac/consortium). Funding for the DPAC has been provided by national institutions, in particular the institutions participating in the *Gaia* Multilateral Agreement. E.G.A. acknowledge support from the Spanish Ministery for Science, Innovation, and Universities through projects AYA-2016-79425-C3-1/2/3-P, AYA2015-69350-C3-2-P, ESP2017-87676-C5-2- R, ESP2017-87143-R. The Centro de Astrobiología (CAB, CSIC-INTA) is a Center of Excellence "Maria de Maeztu". A.P. acknowledges support from ASI-INAF agreement 2018-22-HH.0 *Partecipazione alla fase B1 della missione ARIEL*. We acknowledge support from the Accordo Attuativo ASI-INAF n. 2018.22.HH.O, Partecipazione alla fase B1 della missione Ariel (ref. G. Micela). A.S., M.Pi. acknowledge the financial contribution from the agreement ASI-INAF n.2018-16-HH.0. M.P., I.R. acknowledge support from the Spanish Ministry of Science and Innovation and the European Regional Development Fund through grant PGC2018-098153-B-C33, as well as the support of the Generalitat de Catalunya/CERCA programme. J.I.G.H. acknowledges financial support from Spanish MICINN under the 2013 Ramón y Cajal program RYC-2013-14875. A.S.M. acknowledges financial support from the Spanish Ministry of Science and Innovation (MICINN) under the 2019 Juan de la Cierva Programme. B.T.P. acknowledges Fundación La Caixa for the financial support received in the form of a Ph.D. contract. J.I.G.H., R.R., A.S.M., B.T.P. acknowledge financial support from the Spanish MICINN AYA2017-86389-P.

References

Affer, L., Damasso, M., Micela, G., et al. 2019, A&A, 622, A193
Affer, L., Micela, G., Damasso, M., et al. 2016, A&A, 593, A117
Alonso-Floriano, F. J., Morales, J. C., Caballero, J. A., et al. 2015, A&A, 577, A128
Ambikasaran, S., Foreman-Mackey, D., Greengard, L., Hogg, D. W., & O'Neil, M. 2015, IEEE Transactions on Pattern Analysis and Machine Intelligence, 38, 252
Anglada-Escudé, G. & Butler, R. P. 2012, ApJS, 200, 15
Bailer-Jones, C. A. L., Rybizki, J., Fouesneau, M., Mantelet, G., & Andrae, R. 2018, AJ, 156, 58
Berta, Z. K., Irwin, J., Charbonneau, D., Burke, C. J., & Falco, E. E. 2012, AJ, 144, 145
Chen, J. & Kipping, D. 2017, ApJ, 834, 17
Cosentino, R., Lovis, C., Pepe, F., et al. 2012, in Proc. SPIE, Vol. 8446, Ground-based and Airborne Instrumentation for Astronomy IV, 84461V
Cutri, R. M., Skrutskie, M. F., van Dyk, S., et al. 2003, VizieR Online Data Catalog, 2246
Dawson, R. I. & Fabrycky, D. C. 2010, ApJ, 722, 937
Deeming, T. J. 1975, Ap&SS, 36, 137
Delfosse, X., Forveille, T., Perrier, C., & Mayor, M. 1998, A&A, 331, 581
Dressing, C. D. & Charbonneau, D. 2015, ApJ, 807, 45
Espinoza, N., Kossakowski, D., & Brahm, R. 2019, MNRAS, 490, 2262
Foreman-Mackey, D., Agol, E., Ambikasaran, S., & Angus, R. 2017, AJ, 154, 220
Foreman-Mackey, D., Hogg, D. W., Lang, D., & Goodman, J. 2013, PASP, 125, 306
Fulton, B. J., Petigura, E. A., Blunt, S., & Sinukoff, E. 2018, PASP, 130, 044504
Gaia Collaboration, Brown, A. G. A., Vallenari, A., et al. 2018, A&A, 616, A1
Gaia Collaboration, Smart, R. L., Sarro, L. M., et al. 2020, arXiv e-prints, arXiv:2012.02061
Giacobbe, P., Benedetto, M., Damasso, M., et al. 2020, MNRAS, 491, 5216
González-Álvarez, E., Micela, G., Maldonado, J., et al. 2019, A&A, 624, A27
Goodman, J. & Weare, J. 2010, Communications in Applied Mathematics and Computational Science, 5, 65
Jeffreys, H. 1946, Proceedings of the Royal Society of London Series A, 186, 453
Kervella, P., Arenou, F., Mignard, F., & Thévenin, F. 2019, A&A, 623, A72
Kipping, D. M. 2013, MNRAS, 435, 2152
Kopparapu, R. K., Ramirez, R., Kasting, J. F., et al. 2013, ApJ, 765, 131
Kopparapu, R. K., Ramirez, R. M., SchottelKotte, J., et al. 2014, ApJ, 787, L29
Kreidberg, L. 2015, PASP, 127, 1161
Leto, G., Pagano, I., Buemi, C. S., & Rodono, M. 1997, A&A, 327, 1114
Liddle, A. R. 2007, MNRAS, 377, L74
Lovis, C. & Pepe, F. 2007, A&A, 468, 1115
Luyten, W. J. 1979, LHS catalogue. A catalogue of stars with proper motions exceeding 0"5 annually
Maldonado, J., Affer, L., Micela, G., et al. 2015, A&A, 577, A132
Maldonado, J., Scandariato, G., Stelzer, B., et al. 2017, A&A, 598, A27
Mortier, A., Faria, J. P., Correia, C. M., Santerne, A., & Santos, N. C. 2015, A&A, 573, A101
Osten, R. A., Hawley, S. L., Allred, J. C., Johns-Krull, C. M., & Roark, C. 2005, ApJ, 621, 398

Perger, M., Anglada-Escudé, G., Ribas, I., et al. 2020, arXiv e-prints, arXiv:2012.01862
Perger, M., García-Piquer, A., Ribas, I., et al. 2017, A&A, 598, A26
Pinamonti, M., Damasso, M., Marzari, F., et al. 2018, A&A, 617, A104
Queloz, D., Henry, G. W., Sivan, J. P., et al. 2001, A&A, 379, 279
Reiners, A., Joshi, N., & Goldman, B. 2012, AJ, 143, 93
Reiners, A., Zechmeister, M., Caballero, J. A., et al. 2018, A&A, 612, A49
Robertson, P., Mahadevan, S., Endl, M., & Roy, A. 2014, Science, 345, 440
Scandariato, G., Maldonado, J., Affer, L., et al. 2017, A&A, 598, A28
Schweitzer, A., Passegger, V. M., Cifuentes, C., et al. 2019, A&A, 625, A68
Smith, A. M. S. & WASP Consortium. 2014, Contributions of the Astronomical Observatory Skalnate Pleso, 43, 500
Smith, J. C., Stumpe, M. C., Van Cleve, J. E., et al. 2012, PASP, 124, 1000
Sokal, A. 1996, in Monte Carlo Methods in Statistical Mechanics: Foundations and New Algorithms Note to the Reader
Sozzetti, A., Bernagozzi, A., Bertolini, E., et al. 2013, in European Physical Journal Web of Conferences, Vol. 47, European Physical Journal Web of Conferences, 03006
Stumpe, M. C., Smith, J. C., Catanzarite, J. H., et al. 2014, PASP, 126, 100
Suárez Mascareño, A., González Hernández, J. I., Rebolo, R., et al. 2017, A&A, 605, A92
Suárez Mascareño, A., Rebolo, R., González Hernández, J. I., et al. 2018, A&A, 612, A89
Tuomi, M., Jones, H. R. A., Barnes, J. R., Anglada-Escudé, G., & Jenkins, J. S. 2014, MNRAS, 441, 1545
Zechmeister, M. & Kürster, M. 2009, A&A, 496, 577

Appendix A: Tables

Table A.2. Priors used for the S-index model with `juliet`.

Parameter	Prior	Unit	Description
		S-index parameters	
γ_0	$\mathcal{U}$(-10, 10)	ms^{-1}	zero point for S-index
σ	$\mathcal{LU}$(0.01, 10)	ms^{-1}	Extra jitter term for S-index
		GP parameters	
σ_{GP}	$\mathcal{U}$(0, 20)	ms^{-1}	Amplitude of the GP for the S-index
α_{GP}	$\mathcal{LU}$ (10^{-5}, 1)	d^{-2}	Inverse (squared) length-scale of the external parameter
Γ_{GP}	$\mathcal{LU}$(0.01, 100)	...	Amplitude of the sine-part of the kernel
$P_{rot,GP}$	$\mathcal{U}$(1, 500)	d	Period of the GP quasi-periodic component for the S-index

Notes. The prior labels of $\mathcal{U}$ and $\mathcal{LU}$ represent uniform and loguniform distribution, respectively.

Table A.3. Priors used for GJ 720 Ab fitting the RV+GP model with `juliet`. The model statistically prefered and used to determine the final planetary orbital parameters.

Parameter	Prior	Unit	Description
		RV parameters	
γ_0	$\mathcal{U}$(-10, 10)	ms^{-1}	RV zero point for HARPS-N
σ	$\mathcal{U}$(0.01, 10)	ms^{-1}	Extra jitter term for HARPS-N
		GP parameters	
$\sigma_{GP,RV}$	$\mathcal{U}$(0, 10)	ms^{-1}	Amplitude of the GP for the RVs
$\alpha_{GP,RV}$	$\mathcal{J}$ (10^{-11}, 10^{-6})	d^{-2}	Inverse (squared) length-scale of the external parameter
$\Gamma_{GP,RV}$	$\mathcal{J}$(0.01, 100)	...	Amplitude of the sine-part of the kernel
$P_{rot,GP,RV}$	$\mathcal{U}$(30, 50)	d	Period of the GP quasi-periodic component for the RVs
		Planet parameters	
P	$\mathcal{N}$ (19.5, 0.5)	d	Period of planet b
T_0 (BJD-2,456,400)	$\mathcal{U}$ (0,15)	d	Time of periastron passage
e	$\mathcal{U}$ (0, 0.8)	...	Orbital eccentricity of planet b
ω	$\mathcal{U}$ (0, 360)	deg	Periastron angle of planet b
K	$\mathcal{U}$ (0, 10)	ms^{-1}	RV semi-amplitude of planet b

Notes. The prior labels of $\mathcal{N}$, $\mathcal{U}$ and $\mathcal{J}$ represent normal, uniform, and jeffrey distribution, respectively. The reference time for T_0 is BJD-2,456,400.

Table A.4. Summary of all hyperparameters of the different models applied to GJ 720 A RVs implemented with `juliet` with their corresponding priors and uncertainties.

	σ_{GP} (ms^{-1})	α_{GP} (d^{-2})	Γ_{GP} ...	$P_{rot,GP}$ (d)	P (d)	T_0 (BJD)	e ...	ω (deg)	K (ms^{-1})
BM+GP	$\mathcal{U}$(0, 15)	$\mathcal{J}$ (10^{-20}, 10^{-5})	$\mathcal{J}$(0.01, 100)	$\mathcal{U}$(1, 1000)	...	...	...	...	...
BM+GP+LT*	$\mathcal{U}$(0, 15)	$\mathcal{J}$ (10^{-20}, 10^{-3})	$\mathcal{J}$(0.01, 15)	$\mathcal{U}$(1, 1000)	...	...	...	...	...
BM+1pl	...	...	...	...	$\mathcal{U}$ (1, 50)	$\mathcal{U}$ (0,50)	$\mathcal{U}$ (0, 0.8)	$\mathcal{U}$ (0, 360)	$\mathcal{U}$ (0, 10)
BM+GP+1pl(1)	$\mathcal{U}$(0, 10)	$\mathcal{J}$ (10^{-11}, 10^{-3})	$\mathcal{J}$(0.01, 100)	$\mathcal{U}$(1, 1000)	$\mathcal{N}$ (19.5, 0.5)	$\mathcal{U}$ (0,15)	$\mathcal{U}$ (0, 0.8)	$\mathcal{U}$ (0, 360)	$\mathcal{U}$ (0, 10)
BM+GP+1pl(2)	$\mathcal{U}$(0, 10)	$\mathcal{J}$ (10^{-11}, 10^{-6})	$\mathcal{J}$(0.01, 100)	$\mathcal{U}$(30, 50)	$\mathcal{N}$ (19.5, 0.5)	$\mathcal{U}$ (0,15)	$\mathcal{U}$ (0, 0.8)	$\mathcal{U}$ (0, 360)	$\mathcal{U}$ (0, 10)
BM+GP+1pl+LT*	$\mathcal{U}$(0, 15)	$\mathcal{J}$ (10^{-20}, 10^{-3})	$\mathcal{J}$(0.01, 100)	$\mathcal{U}$(1, 1000)	$\mathcal{N}$ (19.5, 0.5)	$\mathcal{U}$ (0,15)	$\mathcal{U}$ (0, 0.8)	$\mathcal{U}$ (0, 360)	$\mathcal{U}$ (0, 10)
BM+2pl	...	...	...	...	$\mathcal{N}$ (19.5, 0.5)	$\mathcal{U}$ (0,30)	$\mathcal{U}$ (0, 0.8)	$\mathcal{U}$ (0, 360)	$\mathcal{U}$ (0, 10)
	...	...	...	...	$\mathcal{N}$ (42.1, 0.1)	$\mathcal{U}$ (0,40)	$\mathcal{U}$ (0, 0.8)	$\mathcal{U}$ (0, 360)	$\mathcal{U}$ (0, 10)
BM+GP+2pl	$\mathcal{U}$(0, 15)	$\mathcal{J}$ (10^{-11}, 10^{-3})	$\mathcal{J}$(0.01, 100)	$\mathcal{U}$(1, 1000)	$\mathcal{N}$ (19.5, 0.5)	$\mathcal{U}$ (0,15)	$\mathcal{U}$ (0, 0.8)	$\mathcal{U}$ (0, 360)	$\mathcal{U}$ (0, 10)
	...	...	...	...	$\mathcal{N}$ (42.1, 0.5)	$\mathcal{U}$ (0,50)	...	...	$\mathcal{U}$ (0, 10)

Notes. * The LT hyperparameters are rv_{interc} and rv_{slope} indicating the intercept and slope parameters, respectively. Their priors were set with a uniform distribution, $\mathcal{U}$(-100, 100). (1),(2): The difference between these two models is the prior of the GP P_{rot} parameter. For the first model the P_{rot} was set with a wide prior value (1–1000) d (including all possible RV signals) while the second one was set around the value of the possible rotation period of the star (30–50) d. The prior labels of $\mathcal{N}$, $\mathcal{U}$ and $\mathcal{J}$ represent normal, uniform, and jeffrey distribution, respectively. The reference time for T_0 is BJD-2,456,400. All the models include the BM model that includes the RV zero point and an extra jitter term for the HARPS-N RVs, their hyperparameters and priors value were set as $\mathcal{U}$(-10, 10) and $\mathcal{U}$(0.01, 10), respectively.

Table A.5. Summary of the final parameter values of GJ 720 A for the different models that we followed using `juliet`.

Parameter	S-index (BM+GP)	BM+GP	BM+1pl	BM+GP+1pl$^{(1)}$	BM+GP+1pl$^{(2)}$	BM+2pl	BM+GP+2pl
			Base model (BM)				
γ_0 (m/s)	$0.93^{+0.05}_{-0.04}$	$-0.89^{+2.11}_{-2.71}$	$-0.09^{+0.22}_{-0.22}$	$-0.29^{+1.82}_{-2.31}$	$-0.53^{+2.29}_{-2.55}$	$-0.17^{+0.21}_{-0.21}$	$-0.22^{+0.97}_{-1.32}$
σ (m/s)	$0.03^{+0.003}_{-0.002}$	$1.62^{+0.16}_{-0.14}$	$3.25^{+0.19}_{-0.13}$	$1.47^{+0.14}_{-0.15}$	$0.14^{+0.14}_{-0.13}$	$2.25^{+0.18}_{-0.16}$	$1.59^{+0.18}_{-0.20}$
			GP parameters				
σ_{GP} (m/s)	$0.13^{+0.04}_{-0.03}$	$5.41^{+2.04}_{-1.24}$	...	$4.02^{+2.32}_{-1.19}$	$4.44^{+2.32}_{-1.36}$	...	$2.63^{+1.57}_{-0.63}$
α_{GP} (10^{-6}d^{-2})	$50.1^{+114.5}_{-20.5}$	$0.74^{+0.34}_{-0.30}$	...	$1.62^{+3.38}_{-0.78}$	$1.41^{+1.27}_{-0.64}$	...	$4.31^{+15.05}_{-2.57}$
λ (d) $^{(*)}$	$141.28^{+93.5}_{-220.9}$	$1162.48^{+1360.83}_{-1825.74}$	...	$785.67^{+543.99}_{-1132.28}$	$842.15^{+887.36}_{-1250.0}$	...	$481.68^{+257.77}_{-623.78}$
Γ_{GP}	$0.13^{+0.13}_{-0.06}$	$2.84^{+1.65}_{-1.04}$	...	$1.09^{+1.11}_{-0.54}$	$0.99^{+0.84}_{-0.47}$	...	$0.37^{+7.62}_{-0.33}$
$P_{rot,GP}$ (d)	$36.05^{+1.39}_{-1.44}$	$38.93^{+0.03}_{-0.03}$	...	$35.24^{+0.13}_{-0.12}$	$35.23^{+0.10}_{-0.11}$	...	$113.89^{+381.51}_{-0.43}$
			Planet 1 parameters				
P (d)	...	...	$19.484^{+0.007}_{-0.006}$	$19.467^{+0.006}_{-0.006}$	$19.466^{+0.005}_{-0.005}$	$19.486^{+0.006}_{-0.007}$	$19.475^{+0.006}_{-0.006}$
T_0 (d)	...	...	$26.57^{+0.53}_{-0.43}$	$6.80^{+0.45}_{-0.45}$	$6.81^{+0.43}_{-0.42}$	$24.38^{+1.32}_{-18.67}$	$6.42^{+0.44}_{-0.42}$
e	...	...	$0.16^{+0.04}_{-0.04}$	$0.12^{+0.05}_{-0.06}$	$0.12^{+0.05}_{-0.06}$	$0.09^{+0.07}_{-0.06}$	$0.12^{+0.06}_{-0.06}$
ω (deg)	...	...	$169.69^{+37.78}_{-33.43}$	$110.71^{+23.12}_{-24.01}$	$110.22^{+23.97}_{-24.28}$	$114.60^{+37.25}_{-52.62}$	$101..23^{+24.91}_{-26.31}$
K (m/s)	...	...	$3.97^{+0.27}_{-0.37}$	$4.70^{+0.28}_{-0.30}$	$4.72^{+0.27}_{-0.27}$	$3.81^{+0.29}_{-0.31}$	$4.10^{+0.28}_{-0.27}$
			Planet 2 parameters				
P (d)	...	...	...	...	...	$42.11^{+0.04}_{-0.03}$	$42.10^{+0.06}_{-0.06}$
T_0 (d)	...	...	...	...	...	$37.02^{+1.84}_{-2.08}$	$7.55^{+39.88}_{-3.28}$
e	...	...	...	...	...	...	...
ω (deg)	...	...	...	...	...	...	...
K (m/s)	...	...	...	...	...	$2.16^{+0.32}_{-0.31}$	$1.51^{+0.31}_{-0.29}$

Notes. $^{(1),(2)}$: The difference between these two models is the prior of the GP P_{rot} parameter. For the first model the P_{rot} was set with a wide prior value (1–1000) d (including all possible RV signals) while the second one was set around the value of the possible rotation period of the star (30–50) d. $^{(*)}$: The λ parameter corresponds with the length-scale of the GP kernel expressed in day units, it was derived from α_{GP} parameter. The reference time for T_0 is BJD-2,456,400.

Table A.6. Same as for Tab A.3 but for `emcee` instead of `juliet`. Parameters e and ω are derived from the explored parameters $\sqrt{e}sin(\omega)$ and $\sqrt{e}cos(\omega)$

Parameter	Prior	Unit	Description
	RV parameters		
γ_0	$\mathcal{U}$(-10, 10)	ms^{-1}	RV zero point for HARPS-N
σ	$\mathcal{U}$(0.01, 10)	ms^{-1}	Extra jitter term for HARPS-N
	GP parameters		
$B_{GP,RV}$	$\mathcal{LU}(10^{-2}, 100)$	ms^{-1}	Amplitude of the GP for the RVs
$C_{GP,RV}$	$\mathcal{LU}(10^{-2}, 100)$	...	Additive factor impacting on the amplitude of the GP for the RVs
$L_{GP,RV}$	$\mathcal{LU}(300, 10^5)$	d	Length-scale of exponential part of the GP for the RVs
$P_{rot,GP,RV}$	$\mathcal{LU}$(30, 50)	d	Period of the GP quasi-periodic component for the RVs
	Planet parameters		
P	$\mathcal{U}$ (5, 25)	d	Period of planet b
T_0 (BJD-2,456,400)	$\mathcal{U}$ (0,15)	d	Time of periastron passage
e	$\mathcal{U}$ (0, 0.8)	...	Orbital eccentricity of planet b
ω	$\mathcal{U}$ (0, 360)	deg	Periastron angle of planet b
K	$\mathcal{U}$ (0, 10)	ms^{-1}	RV semi-amplitude of planet b

Notes. The prior labels of $\mathcal{U}$ and $\mathcal{LU}$ represent uniform and loguniform distribution, respectively. The reference time for T_0 is BJD-2,456,400.

Table A.1. GJ 720 A data of the HARPS-N observations.

BJD-2,400,000 (d)	RV ($m\,s^{-1}$)	eRV ($m\,s^{-1}$)	NaD1	NaD2	S-index	eS-index	Hα
56438.6283	0.8556	0.6549	0.4531	0.5853	0.8289	0.0040	0.8039
56440.6376	-3.0450	0.9396	0.4540	0.5840	0.7878	0.0057	0.8023
56442.6065	-0.0730	0.8321	0.4523	0.5840	0.8007	0.0046	0.8051
56443.5709	-5.4419	0.7409	0.4533	0.5829	0.7591	0.0062	0.8028
56444.5464	-2.4062	0.6942	0.4512	0.5831	0.7791	0.0046	0.8079
56484.4726	-4.1991	0.8349	0.4519	0.5888	0.7657	0.0053	0.8061
56486.5896	-5.7892	0.7041	0.4510	0.5850	0.7548	0.0049	0.8076
56508.5780	-3.9796	0.9532	0.4535	0.5896	0.8557	0.0057	0.8139
56509.5798	-5.1460	0.6858	0.4538	0.5920	0.8653	0.0056	0.8165
56533.4210	-3.4373	0.6672	0.4526	0.5808	0.7794	0.0043	0.8148
56534.4324	-3.1517	0.8646	0.4521	0.5777	0.7576	0.0057	0.8160
56534.4956	-3.6094	0.8079	0.4527	0.5813	0.7601	0.0055	0.8154
56535.3663	-0.7889	0.8062	0.4536	0.5817	0.7703	0.0058	0.8163
56535.5215	-1.0090	0.6777	0.4540	0.5827	0.7667	0.0044	0.8183
56775.6149	2.1136	1.1157	0.4573	0.5882	0.7240	0.0097	0.8042
56786.6700	-3.5345	0.9845	0.4556	0.5865	0.7900	0.0082	0.8053
56787.5918	-0.7065	0.8225	0.4532	0.5868	0.7936	0.0065	0.8051
56792.5339	0.7418	1.0174	0.4581	0.5968	0.8337	0.0089	0.8063
56811.6383	4.0310	0.7325	0.4548	0.5843	0.8468	0.0056	0.8068
56854.5890	-1.4405	0.6970	0.4545	0.5847	0.8607	0.0049	0.7978
56857.5711	-5.7692	0.6496	0.4560	0.5840	0.8697	0.0051	0.7942
56858.5186	-4.3603	0.6858	0.4541	0.5831	0.8706	0.0052	0.7956
56859.5271	-4.2436	0.8009	0.4556	0.5878	0.8678	0.0061	0.7987
56860.4789	-3.9977	0.5824	0.4533	0.5858	0.8787	0.0045	0.7977
56861.4923	-1.4096	0.6056	0.4551	0.5822	0.8802	0.0048	0.7990
56874.4739	-0.7580	0.6499	0.4574	0.5857	0.9098	0.0054	0.8053
56875.4972	-5.1943	1.2135	0.4579	0.5935	0.9659	0.0111	0.8055
56876.4863	-4.0069	0.9428	0.4556	0.6003	0.9463	0.0088	0.8065
56877.4838	-2.8328	0.7407	0.4535	0.5906	0.8995	0.0054	0.8052
57113.6697	-4.0459	0.8306	0.4570	0.5831	0.9115	0.0076	0.7976
57114.7286	-5.8965	0.9335	0.4707	0.6021	0.8533	0.0102	0.7974
57137.6987	0.4611	0.9086	0.4530	0.5858	0.8346	0.0055	0.8006
57139.7151	4.5178	0.6327	0.4541	0.5843	0.8100	0.0056	0.8001
57142.7166	7.4822	0.7658	0.4531	0.5882	0.8188	0.0055	0.8001
57143.6682	3.3888	0.6213	0.4551	0.5875	0.8208	0.0054	0.8030
57144.6615	3.1809	0.6798	0.4544	0.5884	0.8250	0.0070	0.8005
57145.6867	3.1437	0.8123	0.4609	0.6055	0.8232	0.0077	0.8018
57147.7393	-1.2659	0.7483	0.4559	0.5908	0.8100	0.0056	0.7980
57148.6849	-5.9414	0.7604	0.4551	0.5869	0.8291	0.0054	0.8006
57170.6373	-6.4304	0.6514	0.4515	0.5838	0.8399	0.0051	0.7952
57172.6821	-2.8096	0.8633	0.4536	0.5842	0.8583	0.0061	0.7997
57173.5731	-1.7334	0.8738	0.4529	0.5811	0.8339	0.0073	0.7938
57175.5927	4.2651	0.6846	0.4558	0.5851	0.7993	0.0071	0.7950
57176.5824	3.0572	0.8997	0.4544	0.5902	0.8487	0.0083	0.7967
57178.6893	2.8957	0.8069	0.4547	0.5901	0.8697	0.0067	0.7984
57204.5383	0.2218	0.6601	0.4560	0.5836	0.9393	0.0060	0.8002
57205.5096	-3.3256	0.8361	0.4544	0.5910	0.8940	0.0060	0.8032
57206.5318	-3.4802	0.8711	0.4560	0.5843	0.9110	0.0061	0.7974
57207.4762	-6.2995	0.7452	0.4554	0.5858	0.8685	0.0059	0.7977
57208.5256	-7.9140	1.0426	0.4540	0.5879	0.8754	0.0079	0.7965
57209.6188	-5.2291	0.9096	0.4550	0.5843	0.8657	0.0075	0.7994
57239.4941	3.8668	0.5425	0.4588	0.5871	0.8993	0.0053	0.8031
57240.4922	4.5738	0.6486	0.4563	0.5931	0.9140	0.0056	0.8084
57241.5110	0.2247	0.9067	0.4559	0.5849	0.8829	0.0067	0.8003
57242.4737	-2.8127	2.1974	0.4697	0.6022	1.4265	0.0286	0.8034
57249.5255	-5.6587	0.6795	0.4543	0.5997	0.8689	0.0068	0.8083
57250.4923	-2.2261	0.9313	0.4574	0.5977	0.8539	0.0081	0.8074
57251.4762	-4.7863	0.6921	0.4537	0.5836	0.8432	0.0047	0.8043
57258.4289	3.9843	0.6944	0.4574	0.5842	0.8789	0.0057	0.8035
57259.4298	2.5805	0.7458	0.4564	0.5818	0.8292	0.0054	0.8045
57260.4874	2.0615	0.6685	0.4554	0.5866	0.9011	0.0047	0.8092
57261.4934	1.1212	0.7153	0.4549	0.5852	0.9128	0.0050	0.8062
57262.4796	-0.0115	0.8523	0.4569	0.5874	0.9662	0.0070	0.8159
57263.4798	1.6670	0.6632	0.4551	0.5940	0.9088	0.0058	0.8124
57264.4790	-1.3328	0.7019	0.4562	0.5945	0.9352	0.0068	0.8138
57274.4658	0.7708	0.8334	0.4590	0.5897	0.9777	0.0070	0.8094
57275.4619	3.2613	0.6845	0.4554	0.5897	0.9435	0.0061	0.8090
57276.4603	4.8241	0.6564	0.4589	0.5960	0.9247	0.0059	0.8089
57277.4582	4.7622	0.6351	0.4571	0.5861	0.8972	0.0049	0.8062
57282.4744	4.7420	1.1354	0.4568	0.5829	0.8610	0.0052	0.8058
57285.4754	-5.3744	0.9515	0.4560	0.5917	0.8352	0.0085	0.8122
57286.4849	-5.3450	0.7508	0.4552	0.5878	0.8516	0.0065	0.8086
57287.4630	-5.0051	0.7946	0.4536	0.5888	0.8447	0.0063	0.8086
57290.5193	-1.8430	0.7608	0.4559	0.5891	0.8549	0.0078	0.8091
57291.4861	-2.2635	0.7752	0.4553	0.5888	0.8829	0.0074	0.8090
57293.4607	0.0000	0.6706	0.4566	0.5860	0.8294	0.0072	0.8046
57294.4756	4.9841	1.0672	0.4635	0.5879	0.9403	0.0106	0.8086
57296.4301	9.1730	1.1774	0.4638	0.5932	0.9673	0.0102	0.8110
57303.4081	-0.2229	0.7379	0.4581	0.5862	0.9215	0.0057	0.8080
57472.7269	4.6796	1.1044	0.4591	0.5887	0.8474	0.0100	0.8155
57474.7285	6.5082	0.6286	0.4566	0.5919	0.8705	0.0054	0.8169
57475.7086	7.2436	0.9217	0.4597	0.5860	0.8609	0.0074	0.8144

Table A.1. continued.

BJD-2,400,000 (d)	RV ($m\,s^{-1}$)	eRV ($m\,s^{-1}$)	NaD1	NaD2	S-index	eS-index	Hα
57607.5019	3.7040	1.1875	0.4580	0.5956	0.8568	0.0088	0.8154
57608.4638	2.4916	0.7224	0.4571	0.5901	0.8072	0.0053	0.8145
57609.5581	4.0824	1.6268	0.4688	0.5973	0.8372	0.0141	0.8139
57935.6549	-0.6930	0.9038	0.4557	0.5903	0.9079	0.0075	0.8024
57936.5276	1.5962	0.8964	0.4561	0.5887	0.9448	0.0088	0.8086
57944.5151	2.8329	0.5128	0.4561	0.5854	0.9470	0.0057	0.8103
57971.3846	-2.5676	0.8980	0.4538	0.5881	0.9127	0.0064	0.8089
57974.4582	1.8452	0.8170	0.4566	0.5925	0.8635	0.0068	0.8069
57977.4881	4.2857	0.8850	0.4567	0.5961	0.9621	0.0075	0.8117
57978.4393	5.6847	0.7480	0.4568	0.5924	0.9582	0.0056	0.8090
57979.4464	8.4808	0.7172	0.4584	0.5886	0.9438	0.0049	0.8094
57980.4294	5.6384	0.8731	0.4603	0.5888	0.9438	0.0061	0.8128
57981.4270	7.7884	0.8546	0.4583	0.5875	0.9166	0.0066	0.8077
57982.4171	4.5221	1.0451	0.4610	0.5958	1.0005	0.0082	0.8147
57984.4080	1.2098	0.7717	0.4566	0.5879	0.9227	0.0053	0.8092
57989.3714	-3.6573	0.9132	0.4568	0.5953	0.8604	0.0068	0.8169
57993.4588	0.5419	0.6713	0.4556	0.5913	0.9000	0.0068	0.8187
57996.4369	4.6074	1.0328	0.4587	0.5883	0.8542	0.0078	0.8111
58000.4093	6.8929	1.0264	0.4588	0.5911	0.8793	0.0079	0.8115
58005.4765	-5.8464	0.8280	0.4576	0.5943	0.9780	0.0066	0.8109
58006.4841	-3.9495	0.8971	0.4567	0.5937	0.9824	0.0070	0.8091
58007.4650	-7.5220	0.8376	0.4588	0.5879	0.9833	0.0068	0.8083
58008.4648	-3.2108	0.8609	0.4584	0.5904	0.9610	0.0051	0.8108
58009.4755	-4.3398	1.1500	0.4658	0.5906	1.0225	0.0099	0.8064
58010.4846	-4.2457	0.7485	0.4620	0.5900	1.0320	0.0077	0.8192
58022.3695	-0.2366	0.7895	0.4590	0.5898	0.9144	0.0056	0.8119
58024.4562	-1.6361	0.9246	0.4585	0.5894	0.9257	0.0061	0.8126
58026.3661	-4.9618	0.7807	0.4570	0.5847	0.8861	0.0051	0.8122
58031.4482	-4.1795	0.8973	0.4598	0.5856	0.8790	0.0077	0.8130
58037.4262	1.8943	1.1604	0.4631	0.5910	0.9526	0.0096	0.8099
58044.3890	-4.5156	0.9186	0.4606	0.5879	0.9441	0.0062	0.8091
58333.5067	2.5931	0.7935	0.4628	0.5866	1.0021	0.0059	0.8091
58334.5021	1.1240	0.8291	0.4598	0.5887	0.9903	0.0056	0.8092
58335.4729	-0.0012	1.8726	0.4696	0.6122	1.0690	0.0157	0.8101
58403.3701	4.3495	0.9156	0.4615	0.5880	1.0956	0.0069	0.8172
58406.3686	7.5291	0.7414	0.4633	0.5913	1.0581	0.0065	0.8145
58700.5049	8.2617	1.3557	0.4645	0.5901	1.1238	0.0127	0.8034
58700.5160	6.8301	1.7573	0.4668	0.5946	1.1076	0.0163	0.8053
58724.4723	2.4381	0.8577	0.4606	0.5944	1.1096	0.0064	0.8098
58725.4676	1.6989	0.8991	0.4608	0.5916	1.0699	0.0071	0.8037
58791.3321	6.0912	1.4268	0.4631	0.5969	1.1541	0.0095	0.8232
58792.3266	6.2628	1.1013	0.4653	0.5944	1.0891	0.0081	0.8185
59037.4711	-1.3563	1.0557	0.4621	0.5970	1.0555	0.0073	0.8157
59038.5999	-1.8614	1.3793	0.4637	0.5986	1.1123	0.0096	0.8177
59039.6133	2.4374	1.0650	0.4580	0.6015	1.1118	0.0065	0.8198
59040.6150	2.8533	1.1285	0.4604	0.6013	1.1343	0.0093	0.8190
59068.5029	7.2526	0.9858	0.4603	0.5966	1.1570	0.0077	0.8207
59069.5561	2.5671	0.7651	0.4594	0.5999	1.1577	0.0068	0.8256
59070.5927	4.8134	0.7815	0.4610	0.5930	1.1337	0.0066	0.8220
59072.5652	9.1256	0.8643	0.4634	0.5926	1.2270	0.0074	0.8355